AIAA JOURNAL
Vol. 32, No. 5, May 1994

Monte Carlo Computation of Nonequilibrium Flow in a Hypersonic Iodine Wind Tunnel

Iain D. Boyd*
Cornell University, Ithaca, New York 14853
and
Gerald C. Pham-Van-Diep† and E. Phil Muntz‡
University of Southern California, Los Angeles, California 90089

The nonequilibrium flow formed by the interaction of a freejet of iodine vapor impinging on a blunt body is investigated using numerical and experimental techniques. The computational approach employs the direct simulation Monte Carlo method. The experimental measurements consist of rotational temperature obtained along the flow axis and include portions of both the freejet expansion and blunt-body shock for four different stagnation conditions. Direct comparisons of the numerical results and the experimental data are quite successful at moderate temperatures. Hence, the rotational collision time of iodine is estimated in the temperature range of 100–500 K. At higher temperatures, the agreement between simulation and measurement is less satisfactory. This demonstrates the requirement for the development of a more detailed approach to simulating rotational nonequilibrium in high-temperature flows of diatomic species.

Introduction

AEROSPACE vehicles traveling at hypersonic speed and at high altitude produce flowfields that are in thermochemical nonequilibrium. Many years of both experimental and numerical research have been spent in the study of these flows. Detailed experimental study of hypersonic flows of air requires the latest optical diagnostic techniques. However, even when these are available, it is difficult to reproduce in ground-based facilities the high-enthalpy flow conditions experienced in flight. In the literature, there are very few experimental studies indeed that have provided much insight into the coupled physical relaxation phenomena characteristic of low-density hypersonic flow. This lack of data has severely restricted the development of more sophisticated numerical techniques and models for computing such flowfields. Therefore there exists a very real and urgent requirement for detailed experimental investigation, and accompanying numerical analysis, of hypersonic flows in thermochemical nonequilibrium.

It has been proposed[1] that iodine represents a convenient model gas for investigation of hypersonic nonequilibrium flow phenomena. This is mainly due to the lower characteristic temperatures for vibration and dissociation of iodine in comparison with the diatomic constituents of air. A significant degree of thermochemical nonequilibrium is therefore observed at relatively low enthalpies. This feature of iodine presents promising possibilities for detailed experimental investigation in ground-based facilities using modern optical diagnostic techniques. A pilot scale hypersonic wind tunnel that operates on pure iodine vapor has been designed and tested at the University of Southern California.[2] A preliminary set of rotational temperature measurements for a freejet of iodine impinging on a blunt body was reported in Ref. 2. This flow represents an interesting configuration as the gas first expands from the orifice and is then compressed by the blunt body. Therefore, any numerical approach must successfully simulate each of these important flow phenomena.

A powerful numerical technique for computing low-density nonequilibrium flows is the direct simulation Monte Carlo method (DSMC). This method offers unique opportunities for simulating in great detail the thermochemical nonequilibrium that occurs in the flows of interest. In previous studies, successful comparisons between DSMC and experimentally measured distributions for velocity[3] and rotational energy[4] have been made. The main purpose of the present paper is to make a comparison of numerical results obtained using the DSMC technique and new experimental data for rotational temperature. For application to the iodine wind tunnel, it is necessary to develop the appropriate relaxation constants to be used in the DSMC models. By successful comparison with the experimental data, a rotational relaxation time for iodine at low temperatures is estimated. General flowfield properties computed with the DSMC technique are also discussed.

Experimental Facility

The pilot facility operates at a range of stagnation chamber conditions. Two different pressures (30 and 100 Torr) and two different temperatures (773 and 1000 K) are considered. Under these conditions the degree of dissociation of iodine is less than 5%. The four different cases examined in this study are listed in Table 1. The iodine vapor is expanded through an orifice with a diameter of 2 mm into a vacuum chamber at a background pressure maintained at 10^{-4} Torr. At a distance of 26 mm from the orifice a 7.25-cm diam disk is located.

Diagnostic Technique

The relative population of I_2 molecules in a given rovibrational state is measured using transient laser induced fluorescence (TLIF). The technique has the advantage of generating strong and easily detectable signals. Moreover, because the excitation is achieved by means of a 30-ns laser pulse, the signal is insensitive to quenching provided the fluorescence is detected during a time gate that is small compared with the local quenching time. The TLIF technique used in this study is described elsewhere.[5,6]

To probe individual rovibrational levels of the molecules composing the flowfield, a narrow-band tunable dye laser excites the I_2 molecules from a rovibrational level (V'', J'') of the ground electronic state $X(^1\Sigma_0)$ to a rovibrational level (V', J') of the $B(^3\Pi_0)$ state. Figure 1 shows the intermolecular potentials of I_2 involved in the fluorescence process. For individual transitions to be excited, the laser line width has to be of the order of 0.05 cm^{-1}. This requires installation of an air-spaced intracavity etalon in the laser

Received Aug. 2, 1993; revision received Nov. 15, 1993; accepted for publication Dec. 4, 1993.

*Assistant Professor, School of Mechanical and Aerospace Engineering. Member AIAA.
†Graduate Assistant, Department of Aerospace Engineering. Member AIAA.
‡Professor, Department of Aerospace Engineering. Fellow AIAA.

Table 1 Total and inlet flow conditions

Case	p_0 ,Torr	T_0, K	γ	ρ_∞, kg/m^3	T_∞, K	M_∞
1	100	1000	1.286	9.24×10^{-3}	339	3.54
2	30	1000	1.320	2.64×10^{-3}	293	3.77
3	100	773	1.310	11.6×10^{-3}	237	3.70
4	30	773	1.325	3.42×10^{-3}	222	3.65

tuning block. Emission spectra are obtained by scanning the laser wavelength, i.e., successively exciting levels of the X state to levels of the B state. The fluorescence signal is observed through a fixed wide spectral window (=20 °A) of a spectrometer whose main purpose is to filter scattered photons at the laser frequency and at the overtones other than the one detected by the spectrometer. In the work described here, the spectrometer is tuned to detect the first overtone, i.e., $\Delta V = V_{\text{final}} - V_{\text{initial}} = +2$. The intensity of the fluorescence signal I_{fluo} is a measure of the population in level (V'', J'') provided the transition strengths for both the absorption (B_{12}) and emission (A_{23}) phases are known. The indices 1, 2, and 3 correspond to the initial lower state, intermediate upper state, and final lower state, respectively. In this study, B_{12} and A_{23} are calculated from radiative decay rates computed by Brewer and Tellinghuisen.[7] Direct dissociation by absorption to the repulsive $^1\Pi_{1u}$ state depletes the population in the probed level (1) and consequently makes saturation of the intermediate level (2) extremely difficult to achieve. Typically, 20% of the absorbed laser energy goes into dissociative reactions.[7] Predissociation of the molecules during the excitation process produces an enhanced decay of the intermediate state. This effect has been investigated by Capelle and Broida,[8] whose measurements of radiative decay rates are used in this study. A detailed description of how both absorption and emission transition strengths are computed can be found in a companion publication.[5] The fluorescence signal I_{fluo} is normalized by laser energy, and the relative population $N(V'', J'')$ is then calculated using

$$N(V'', J'') \propto \frac{I_{\text{fluo}}}{f(B_{12})\, A_{23} SP(J'')} \tag{1}$$

where $SP(J'')$ is a factor that accounts for the nuclear spin of the molecule. It takes a value of 7 if J'' is odd and 5 if J'' is even. The quantity $f(B_{12})$ is a coefficient that quantifies the absorption of the laser radiation by the probed level, dissociation and predissociation of the molecules during the excitation process, and the pulsed nature of the experiment.[5] This quantity is determined by computing the response $N_2(t)$ of the intermediate level (2) to a laser pulse of Gaussian shape with a full width half maximum (FWHM) of 25 ns. The function $N_2(t)$ is subsequently integrated over a time gate of 100 ns during which the fluorescence signal is detected.

The transitions chosen for rotational population measurement are (19, 0) P129, (20, 0) P154, (17, 0) R42, (17, 0) R38, (17, 0) R43, (18, 0) R101, and (17, 0) P39. They require laser excitation at approximately 5683 °A and have been identified previously by means of Fourier spectrometry.[9] Although the selected transitions absorb frequencies in the vicinity of Kr^+ laser lines, chosen transitions are not limited to those corresponding to common lasers. Indeed, Dunham expansion coefficients have been determined for a large number of rovibrational levels for both the X and B states.[10] Consequently, transitions can be chosen judiciously to cover a large number of rotational quantum numbers while requiring small spectral laser scans.[5]

The relative populations in a selected number of rotational levels are analyzed on a Boltzmann plot where $N_1(V'', J'')/(2J''+1)$ is plotted vs $J''(J''+1)$ on a log plot. An example of this is shown in Fig. 2 for the particular case of a stagnation pressure of 100 Torr, a stagnation temperature of 1000 K, and axial positions in the freejet of 5, 10, 20, and 24 mm from the orifice. It is found that the data are easily fitted linearly within experimental errors. Under the assumption that the rotational energy distribution is in equilibrium, a rotational temperature T_{rot} is determined based on the slope S of the best linear fit and the characteristic rotational temperature $\theta_r = 0.053$ K using the expression

$$T_{\text{rot}} = \theta_r / S \tag{2}$$

Numerical Investigation

Near the exit of the orifice, the density is sufficiently large to insure continuum flow. However, the density decays rapidly as the gas expands away from the orifice. The Knudsen number associated with the shock wave formed at the blunt body is therefore relatively large. Because of this low-density nature of the expanding iodine flow, the DSMC technique is an appropriate numerical approach. The DSMC computations begin at a distance of 5 mm from the orifice exit. The computational domain extends to 26 mm along the axis and to 50 mm radially. The disk is 36.25 mm high in

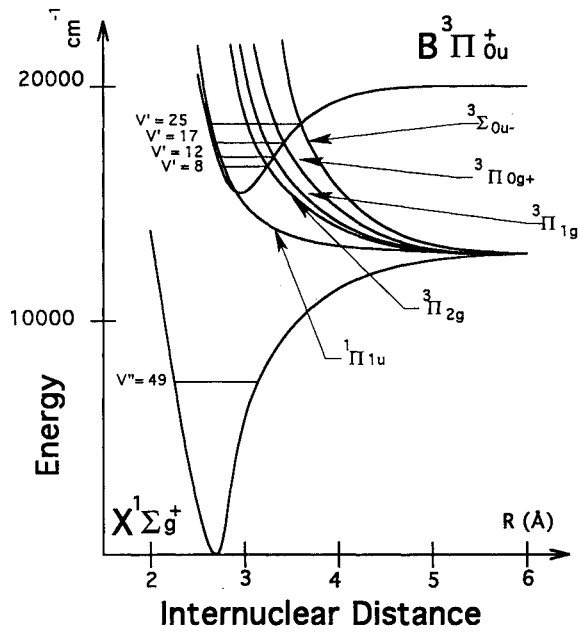

Fig. 1 Intermolecular potentials for I_2 that participate in the fluorescence process.

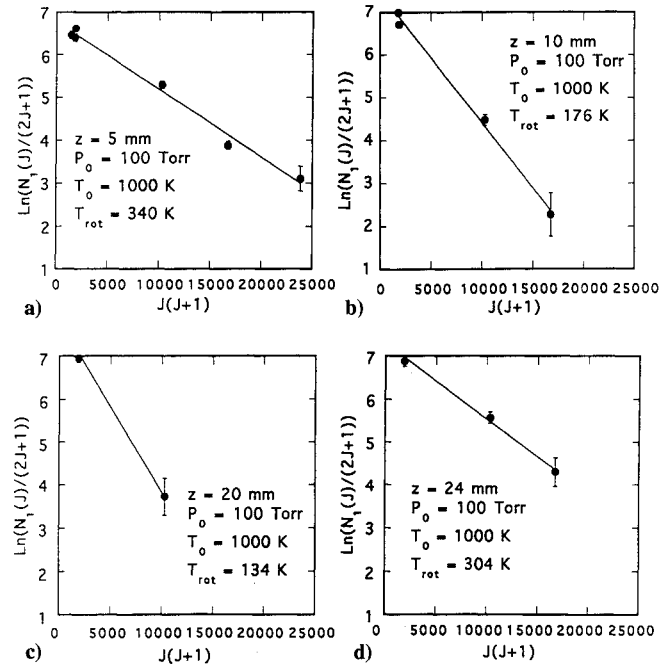

Fig. 2 Boltzmann plots of rotational populations along the jet axis at distances from the orifice of a) 5 mm, b) 10 mm, c) 20 mm, and d) 24 mm.

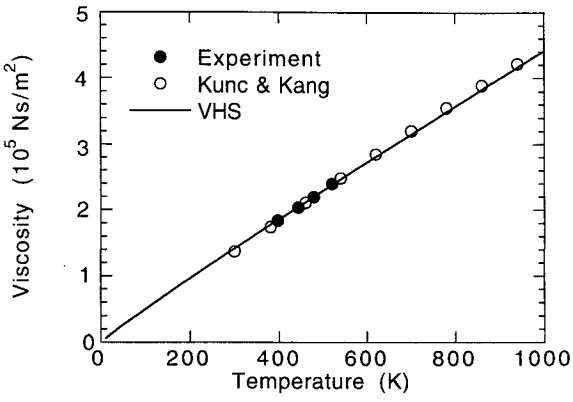

Fig. 3 Temperature dependence for the viscosity coefficient of iodine.

the axisymmetric grid. It is assumed that the surface of the disk is diffusely reflecting with full accommodation to the wall temperature. The disk is made of a ceramic material that will be heated by the compressed gas to an unknown extent. A wall temperature of 400 K is used in all simulations. Except for the inlet plane and the surface of the disk, all other boundaries are treated as expansion into a vacuum.

The flow conditions input to the DSMC code at the upstream boundary are calculated using the theory of Ashkenas and Sherman.[11] In Ref. 11, the Mach number M at a distance x along the axis of a freejet formed from an orifice of diameter D is given by

$$M = A\left(\frac{x-x_0}{D}\right)^{\gamma-1} - \frac{1}{2}\left(\frac{\gamma+1}{\gamma-1}\right)/A\left(\frac{x-x_0}{D}\right)^{\gamma-1} \tag{3}$$

The constants A and x_0 are determined in Ref. 11 for values of the ratio of specific heats $\gamma = 5/3$, 7/5, and 9/7. These values of γ correspond to full equilibration of the translational, rotational, and vibrational modes of a diatomic molecule, respectively. Using the Mach number defined by Eq. (3), together with the isentropic relationships and the stagnation conditions, all fluid properties are obtained as a function of distance along the jet axis. At a fixed distance from the orifice exit, the distribution of density at an angle θ to the axis is described in Ref. 11 by the relation

$$\frac{\rho(\theta)}{\rho(0)} = \cos^{2}\frac{\pi\theta}{2\phi} \tag{4}$$

where ϕ is a constant again evaluated at the three different values for γ. Using the density defined by Eq. (4) and the isentropic relationships, the angular dependence of all properties is evaluated. In this manner, Eqs. (3) and (4) are employed to derive the flow properties at the upstream boundary of the DSMC calculation. For each of the conditions investigated, the value of γ is varied until the temperature on the axis is equal to the experimental measurement of rotational temperature at a distance of 5 mm from the orifice. In general, the values of γ employed in this way are equal to or just greater than 9/7. Thus, in all cases, the gas is close to full vibrational equilibrium at the DSMC inlet plane. Linear interpolation is used to estimate the values of A, x_0, and ϕ required in the previous equations for the values of γ lying between 9/7 and 7/5. Of course, this approach to defining the input flow conditions is approximate. The values of γ employed in each of the four cases considered are listed in Table 1. Also included are the freestream conditions obtained from Eq. (3) on the jet centerline at 5 mm from the orifice.

In the present study, a vectorized DSMC code[12] is employed. This code models two-dimensional axisymmetric flow and includes the effects of translational, rotational, vibrational, and chemical nonequilibrium. For translational nonequilibrium, detailed calculations for the collision cross sections of iodine reported by Kang and Kunc[13] are employed to obtain appropriate parameters in the variable hard sphere (VHS) collision model.[14] Using this approach, it is found that the reference collision diameter is 8.8×10^{-10} m and the viscosity temperature exponent is $\omega = 0.945$ at a reference temperature of 273 K. Comparisons of the variation of viscosity with temperature obtained with these parameters in the VHS model and the detailed calculations of Ref. 13 are shown in Fig. 3. Experimental data points are also included and indicate that the theoretical models are quite accurate. The VHS parameters reveal that iodine has a very large collision diameter and a very soft potential that is close to the ideal Maxwellian molecule.

Rotational nonequilibrium is simulated in the DSMC code using the probability of Boyd[15] that depends on the total energy of each collision ε_c in the following way:

$$\phi_r Z_\infty = 1 + \frac{\Gamma(\zeta+2-\omega)}{\Gamma\left(\zeta+\frac{3}{2}-\omega\right)}\left(\frac{kT^*}{\varepsilon_c}\right)^{\frac{1}{2}}\frac{\pi^{\frac{3}{2}}}{2} + \frac{\Gamma(\zeta+2-\omega)}{\Gamma(\zeta+1-\omega)}\left(\frac{kT^*}{\varepsilon_c}\right)\left(\frac{\pi^2}{4}+2\right) \tag{5}$$

where T^* is a temperature characteristic of the potential of the molecule, Z_∞ is the maximum collision number, and ζ is the average number of degrees of freedom participating in a collision. For iodine, T^* is given in Ref. 16 as 557 K. A search in the literature revealed no previous studies of the rotational relaxation rate of iodine. In the present study, Z_∞ is therefore treated as a free parameter to be determined by comparison of the simulation results with the experimental measurements of rotational temperature.

The expression in Eq. (5) is obtained from a temperature-dependent form for the rotational collision number proposed by Parker.[17,18] In the original analysis, Parker's equation is obtained as a series expansion in T^*/T in which only the first three terms are retained. Similarly, in the derivation of Eq. (5) the same three terms are included. For application to iodine, the value of T^* (=557 K) is much greater than that for other diatomics for which the model was derived (e.g., $T^* = 91$ K for N_2). Therefore, it is considered appropriate to include the next term in Parker's expansion series and thus obtain the following DSMC probability:

$$\phi_r Z_\infty = \text{Eq. (5)} + \frac{\Gamma(\zeta+2-\omega)}{\Gamma\left(\zeta+\frac{1}{2}-\omega\right)}\left(\frac{\pi kT^*}{\varepsilon_c}\right)^{\frac{3}{2}} \tag{6}$$

In Eq. (6), it is necessary to employ a larger value of Z_∞ to be consistent with Eq. (5) at low temperatures.

Analysis of vibrational relaxation in iodine is also included in the DSMC calculation. This subject is discussed in detail in a separate study.[5] For the flow conditions investigated the vibrational temperature is assumed to be in equilibrium with the translational and rotational modes at the inlet plane located at 5 mm from the orifice. This assumption is almost certainly incorrect due to freez-

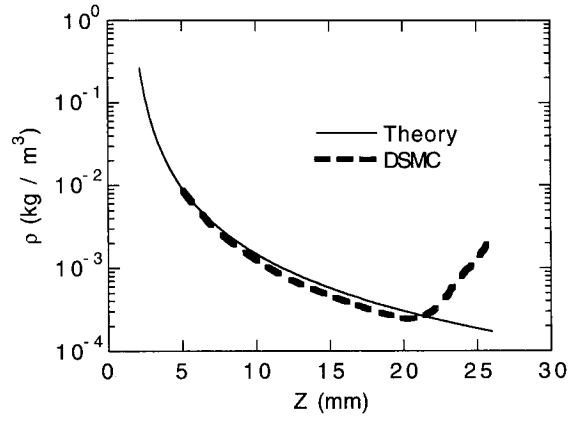

Fig. 4 Comparison of density along the axis predicted by the Ashkenas-Sherman theory and by DSMC for case 1.

ing of the vibrational mode during rapid expansion from the orifice. However, it should not affect the results of the study reported here, which concentrates on rotational relaxation. The DSMC calculations reported in Ref. 5 indicate that no vibrational relaxation occurs at any of the flow conditions investigated. Thus, the vibrational mode is entirely frozen in the computational domain, and any erroneous value assigned at the inlet boundary has no effect on the other flow properties. Dissociation rates for iodine obtained from Davidson[19] are also implemented in the current study. Under the flow conditions investigated, however, no chemical reactions occur.

Results and Discussion

The DSMC simulations reported in this section employ a computational grid that consists of 230 cells axially and 80 cells radially. The topology is nonuniform and accounts for local variation in density. A low-resolution calculation is performed to estimate this variation after which cell sizes are adjusted accordingly. Along the axis, where the densities are highest, the cell lengths are always of the order of one local mean free path. The time step is everywhere constant at a fraction of the average time between collisions in the freestream. Typical simulations employ 500,000 particles. Each calculation is performed over 20,000 iterations before sampling is commenced for a further 5,000 steps. Execution times on a Cray C-90 are of the order of 40 min.

To gain an idea of the flowfields involved in these studies, the high-pressure and high-temperature conditions of case 1 are first considered. One reason for emphasizing this case is the fact that the continuum Ashkenas-Sherman theory is most valid for these conditions. Thus, the data along the DSMC inlet plane located at 5 mm from the orifice should be most accurate. It is also worth noting that the value of γ under these conditions is 9/7, which is that for a gas in vibrational equilibrium. The variation in density along the jet centerline for this case is shown in Fig. 4 and compared with the theory of Ref. 11. It is found that the DSMC solution initially follows the Ashkenas-Sherman theory, then undergoes slightly faster expansion, before the effect of the blunt body starts to form a thick, diffuse shock. Similar trends are observed for the variation in temperature along the axis. Comparison along the axis of theory and the translational temperature computed using DSMC is shown in Fig. 5. Note the very high temperature attained by the gas in the shock. More detailed quantitative comparisons between DSMC and experiment are provided later in this section.

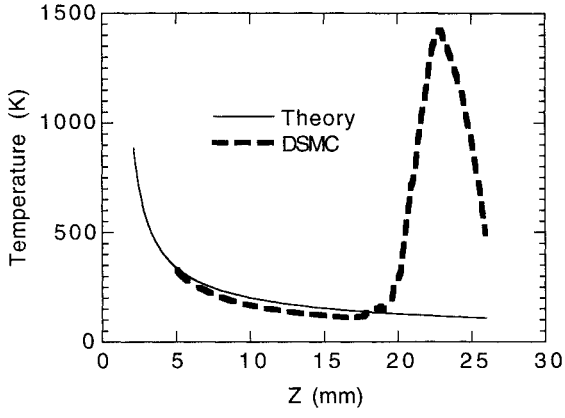

Fig. 5 Comparison of temperature along the axis predicted by the Ashkenas-Sherman theory and by DSMC for case 1.

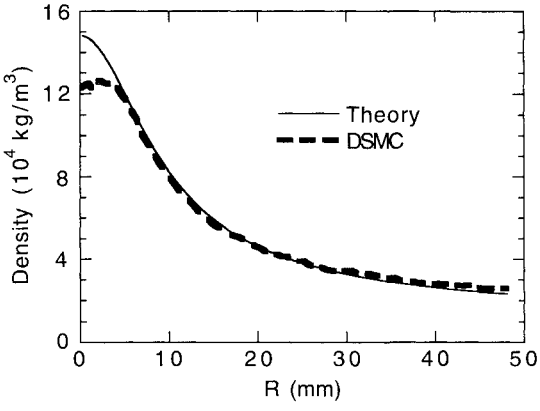

Fig. 6 Comparison of density along the radius at Z = 10 mm predicted by the Ashkenas-Sherman theory and by DSMC for case 1.

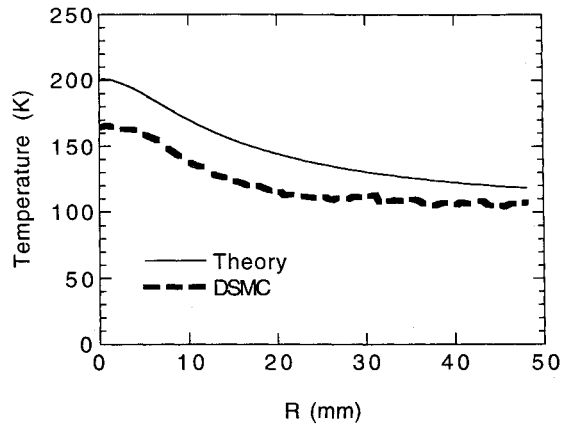

Fig. 7 Comparison of temperature along the radius at Z = 10 m predicted by the Ashkenas-Sherman theory and by DSMC for case 1.

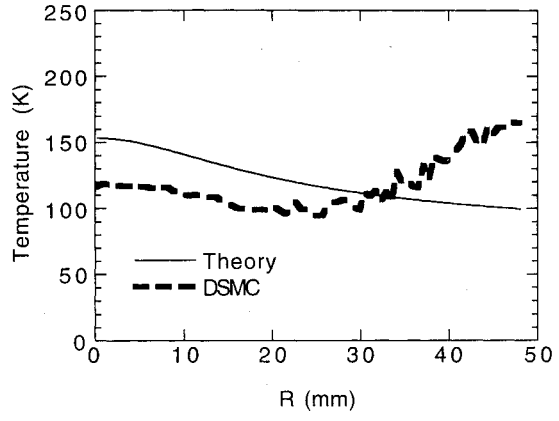

Fig. 8 Comparison of temperature along the radius at Z = 15 m predicted by the Ashkenas-Sherman theory and by DSMC for case 1.

Comparison of theory and DSMC for the radial density profile at an axial distance of 10 mm is shown in Fig. 6. There is generally very good agreement except at small distances from the centerline. The reduction in density with radial distance is evident from this figure. The corresponding comparison for translational temperature is shown in Fig. 7 for the same location. As expected from Fig. 5, the DSMC temperatures are generally lower than the theoretical values. Translational temperatures are again compared in Fig. 8 at the axial coordinate of 15 mm. An interesting structure is observed in the flow at large distances from the axis where an increase in the DSMC temperature is observed. Contours of translational temperature for the entire flowfield are shown in Fig. 9. The shock structure formed in front of the body requires explanation. The decrease in density away from the axis causes a perceptible thickening of the shock in the radial direction. This behavior is also observed in fluorescence images generated in the experimental facility. The increased shock thickness is the structure observed at large radii in Fig. 8. Note that the expansion fan that forms immediately above the vertical plane representing the blunt body is also evident in Fig. 9.

Detailed consideration is next given to the comparison of the DSMC results with the experimental measurements of rotational temperature along the axis. In Fig. 10 the results for case 1 are shown. In this figure, the estimated experimental error bars are

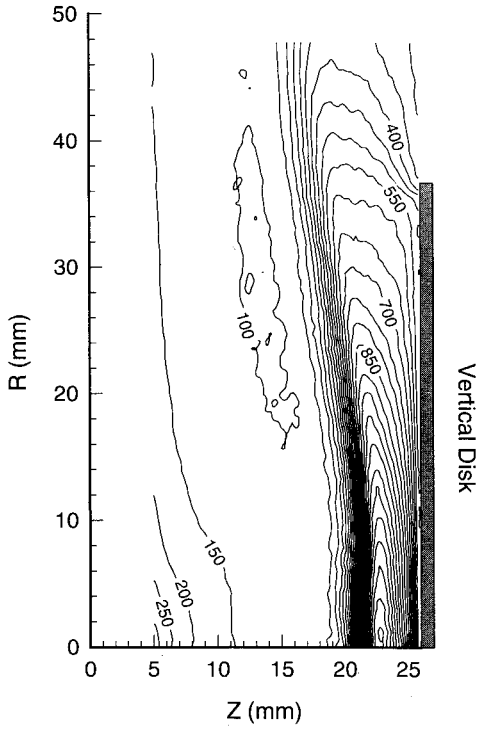

Fig. 9 Flowfield contours of translational temperature computed using DSMC for case 1.

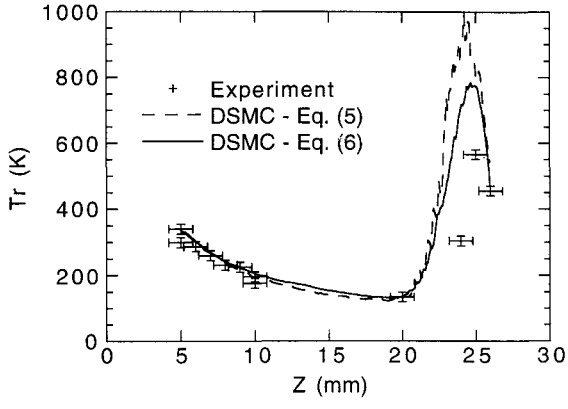

Fig. 10 Comparison of rotational temperatures computed using two different DSMC relaxation models and experimental data along the axis for case 1.

provided. Since these are about the same for all of the cases investigated, they are omitted from all following figures. The two different DSMC results correspond to the use of Eqs. (5) and (6) for simulating the rate of rotational relaxation. For each of the simulations, there is very good agreement obtained in the expansion region of the flowfield. The computed rotational temperatures are in rather poor agreement with the experimental data in the compression region of the flowfield. With either relaxation model, the rise in rotational temperature computed using DSMC is much too rapid. The results are computed using values for Z_∞ of 75 in Eq. (5) and 150 in Eq. (6). Note that a value of $Z_\infty = 50$ is obtained using the theory of Parker.[17] A comparison of the rotational collision numbers obtained using Eqs. (5) and (6) using these values is shown in Fig. 11 as a function of temperature. Note that, at higher temperatures, Eq. (6) gives higher collision numbers, whereas the two models give similar values at lower temperatures.

The translational and rotational temperatures computed using Eq. (6) in DSMC are again compared with the experimental measurements of rotational temperature in Fig. 12. Note the strong degree of thermal nonequilibrium in the shock wave. The comparison indicates that the probability of rotational energy exchange should be smaller at high translational temperatures. The predicted rotational temperatures continue to agree with the experimental data up to the point where the translational temperature increases above a value between 500 and 1000 K. Beyond this point, the calculated rotational temperatures are significantly higher than the measured values.

Comparisons of the rotational temperature measurements taken along the axis with the DSMC results for both translational and rotational temperature are made in Figs. 13–15, respectively, for cases 2–4. The effect of the reduced stagnation pressure in Fig. 13 is to increase the shock thickness and standoff distance considerably. Simultaneously, because of the lower densities, the peak

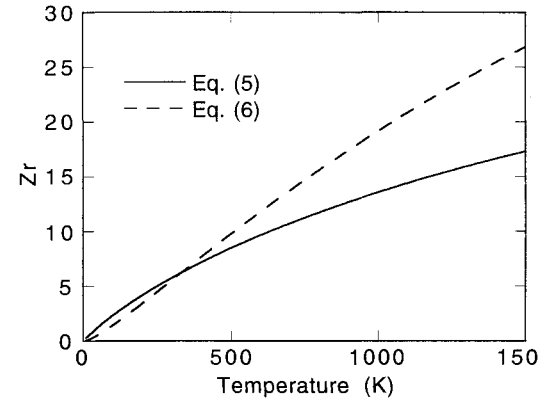

Fig. 11 Comparison of two different DSMC rotational relaxation models for iodine.

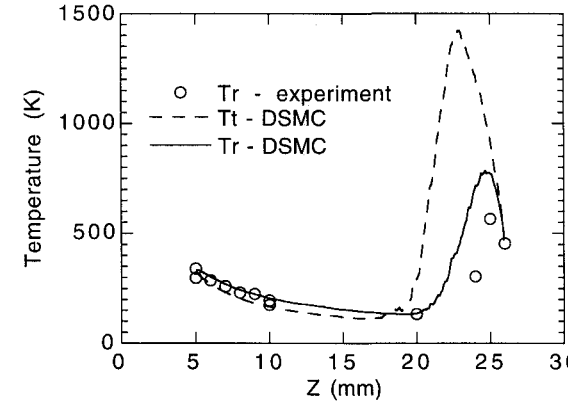

Fig. 12 Comparison of temperatures along the axis obtained experimentally and numerically for case 1.

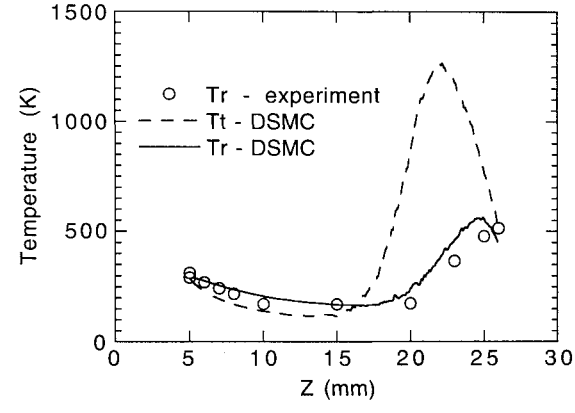

Fig. 13 Comparison of temperatures along the axis obtained experimentally and numerically for case 2.

translational and rotational temperatures are reduced. There is also significantly less rotational relaxation, leading to a higher minimum rotational temperature. The effects of cases 3 and 4 are mainly just direct scaling of the temperature from 1000 to 773 K: however, there are also smaller differences caused by the temperature dependence of the rotational relaxation model employed.

All of these simulations employed Eq. (6) as the rotational relaxation model. In each case, for moderate translational temperatures, the rotational relaxation rate appears to be quite accurately simulated. Significantly, in a similar way to the data compared in Fig. 12, the rotational relaxation model fails in each of Figs. 13–15 when the translational temperature rises above about 500 K. Once the translational temperature increases in the shock front, the simulations compute a rotational relaxation rate that is too high. As observed in Fig. 10, a small improvement in the predicted rotational temperature is obtained by including the extra term in Eq. (6). Clearly, additional terms of this type may improve the simulation results further. However, such analysis is purely speculative. The original theory of Parker does not permit the inclusion of terms beyond Eq. (6), and so they could only be added in an artificial manner. A more satisfactory solution to the problem lies in the development of more detailed rotational relaxation models that account for high-temperature effects. Almost certainly, at these higher translational temperatures, the relaxation of the rotational mode of a diatomic molecule cannot be described by a single rate. The observation that the rotational relaxation rate is slower at high temperatures than the Parker model predicts has also been made recently for nitrogen.[20] The fact that a similar conclusion is drawn here for iodine gives the first evidence that high-temperature nonequilibrium behavior in air may be analyzed qualitatively through the study of alternative molecular species such as iodine.

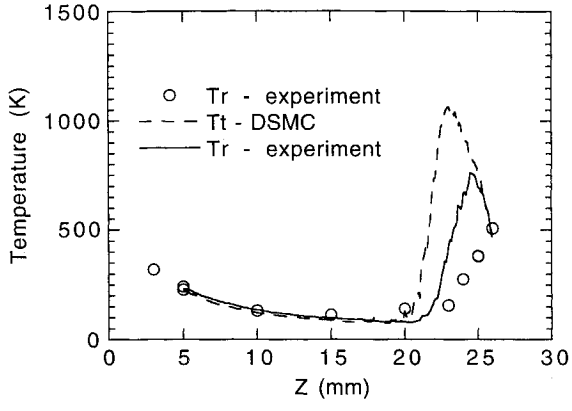

Fig. 14 Comparison of temperatures along the axis obtained experimentally and numerically for case 3.

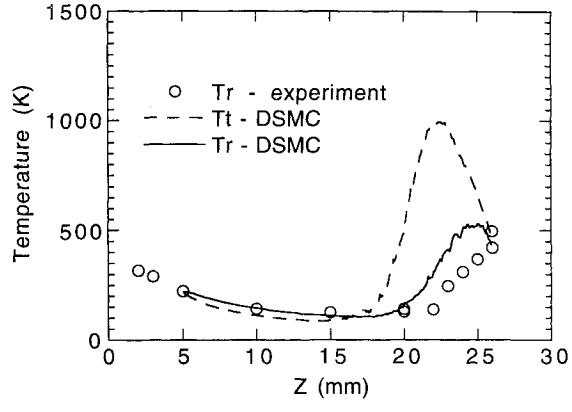

Fig. 15 Comparison of temperatures along the axis obtained experimentally and numerically for case 4.

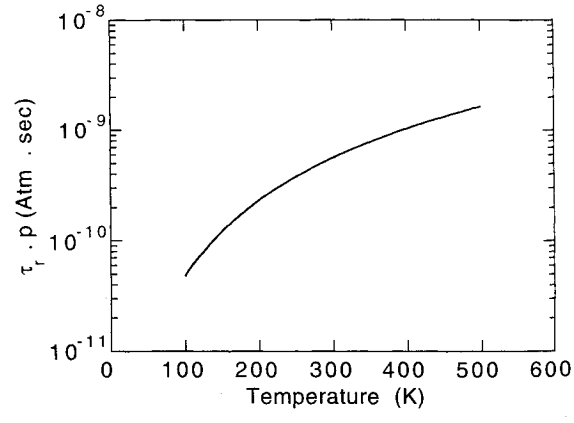

Fig. 16 Temperature dependence of the product of the rotational relaxation time for iodine and the pressure.

The measurements of rotational temperature reported in the current study should be viewed with a certain degree of caution. Further investigations in a larger-scale facility are required for verification of the data. It is also desirable to study flow in a simpler configuration such as a normal shock wave. Nevertheless, it is concluded from the present comparisons of numerical results and experimental data that the rotational relaxation rate of iodine vapor is quite well described by Eq. (6) for the temperature range of 100–500 K. Using the parameters derived earlier for the VHS collision model, the elastic collision time for iodine τ_c may be evaluated as a function of temperature. Then, the rotational collision time τ_r may be derived using the definition

$$\tau_r = Z_r \times \tau_c \tag{7}$$

The rotational relaxation time obtained in this manner when multiplied by pressure (in atmospheres) is shown as a function of temperature in Fig. 16. At higher temperatures, the rotational collision time obtained from Eq. (7) is too small.

As a final note, in all of the calculations performed, the value of the wall temperature is found to have almost no effect on the rise of the rotational temperature in the shock front. This behavior is entirely due to the compression of the gas. The wall temperature does determine the postshock relaxation behavior at small distances from the wall. For the present studies, the value of 400 K is found to give reasonable agreement for each of the four conditions investigated.

Conclusion

Advanced numerical and experimental techniques have been applied to nonequilibrium flows of iodine vapor. Successful comparisons of rotational temperatures obtained with these methods have permitted a rotational relaxation time for iodine to be estimated for the first time. The behavior of iodine at high temperatures indicates that rotational relaxation cannot be described by a single rate under such conditions. This type of behavior almost certainly also occurs in the diatomic species of air. The present study therefore provides a first indication that iodine vapor does represent a model gas that provides experimental access for investigation of thermochemical nonequilibrium phenomena. The detailed measurements obtained in the experimental facility may now be employed for the development of more accurate rotational relaxation models. Investigation in a full-scale facility should be undertaken to verify the data reported here. Through further increases in the stagnation enthalpy, additional studies of vibrational and chemical nonequilibrium in iodine using experimental and numerical methods should yield important information on these processes for diatomic species.

Acknowledgment

Support for the second and third authors by the Air Force Office of Scientific Research, AFOSR-90-0170, is gratefully acknowledged.

References

[1]Kunc, J. A., Muntz, E. P., and Weaver, D. P., "Model Gases for the Detailed Study of Microscopic Chemical Nonequilibrium in Diatomic Gas Flows," AIAA Paper 90-1662, Seattle, WA, June 1990.

[2]Pham-Van-Diep, G. C., Muntz, E. P., Erwin, D. A., and Kunc, J. A., "Measurement of Rotational Temperature in a Free Jet Flow of Chemically Reacting Iodine Vapor," 18th International Symposium on Rarefied Gas Dynamics, Vancouver, Canada, July 1992.

[3]Pham-Van-Diep, G. C., Erwin, D. A., and Muntz, E. P., "Highly Nonequilibrium Molecular Motion in a Hypersonic Shock Wave," *Science*, Vol. 245, Aug. 1989, pp. 624–627.

[4]Boyd, I. D., "Relaxation of Discrete Rotational Energy Distributions Using a Monte Carlo Method," *Physics of Fluids A*, Vol. 5, May 1993, pp. 2278–2286.

[5]Pham-Van-Diep, G. C., Muntz, E. P., and Boyd, I. D., "Measurement of Rotational and Vibrational Population Distributions in a Free-Jet Flow of Chemically Reacting Iodine Vapor and Comparison with Monte Carlo Predictions," AIAA Paper 93-2996, Orlando, FL, July 1993.

[6]Pham-Van-Diep, G. C., "Chemically Reacting, Hypersonic Flows of Iodine Vapor for the Study of Nonequilibrium Phenomena in Diatomic Gases," Ph.D. Thesis, Dept. of Aerospace Engineering, Univ. of Southern California, Los Angeles, CA, Aug. 1993.

[7]Brewer, L., and Tellinghuisen, J., "Quantum Yield for Unimolecular Dissociation of I_2 in the Visible Absorption," *Journal of Chemical Physics*, Vol. 58, 1972, pp. 3929–3938.

[8]Capelle, G. E., and Broida, H. P., "Lifetimes and Quenching Cross Section of I_2," *Journal of Chemical Physics*, Vol. 58, 1972, pp. 4212–4222.

[9]Gerstenkorn, S., and Luc, P., "Assignment of Several Groups of Iodine (I_2) Lines in the B-X System," *Journal of Molecular Spectroscopy*, Vol. 77, 1979, pp. 310–321.

[10]Martin, F., Bacis, R., Churassy, S., and Verges, J., "Laser-Induced-Fluorescence Fourier Transform Spectrometry of the XO_g^+ State of the I_2: Extensive Analysis of the BO_u^+-XO_g^+ Fluorescence Spectrum of $^{127}I_2$," *Journal of Molecular Spectroscopy*, Vol. 116, 1986, pp. 71–100.

[11]Ashkenas, H., and Sherman, F. S., "Structure and Utilization of Supersonic Free Jets in Low Density Wind Tunnels," *4th International Symposium on Rarefied Gas Dynamics*, Academic Press, New York, 1966, pp. 84–105.

[12]Boyd, I. D., and Gökçen, T., "Computation of Axisymmetric Ionized Flows Using Particle and Continuum Methods,"AIAA Paper 93-0729, Reno, NV, Jan. 1993.

[13]Kang, S. H., and Kunc, J. A., "Viscosity of High Temperature Iodine," *Physical Review A*, Vol. 44, Sept. 1991, pp. 3596–3605.

[14]Bird, G. A., "Monte Carlo Simulation in an Engineering Context," *Rarefied Gas Dynamics*, edited by Sam S. Fisher, Vol. 74, Progress in Astronautics and Aeronautics, Part I, AIAA, New York, 1981, pp. 239–255.

[15]Boyd, I. D., "Analysis of Rotational Nonequilibrium in Standing Shock Waves of Nitrogen," *AIAA Journal*, Vol. 28, No. 11, 1990, pp. 1997–1999.

[16]Hirschfelder, J. O., Curtiss, C. F., and Bird, R. B., *Molecular Theory of Gases and Liquids*, Wiley, New York, 1954, p. 1110.

[17]Parker, J. G., "Rotational and Vibrational Relaxation in Diatomic Gases," *Physics of Fluids*, Vol. 2, No. 7, 1959, pp. 449–462.

[18]Parker, J. G., "Comparison of Experimental and Theoretical Vibrational Relaxation Times for Diatomic Gases," *Journal of Chemical Physics*, Vol. 41, No. 9, 1964, pp. 1600–1609.

[19]Davidson, N., *Fundamental Data Obtained from Shock Tube Experiments*, Pergamon, Oxford, England, UK, 1961, p. 138.

[20]Moreau, S., Bourquin, P. Y., Chapman, D. R., and MacCormack, R. W., "Numerical Simulation of Sharma's Shock-Tube Experiment," AIAA Paper 93-0273, Jan. 1993.